Developmental changes in mouse motor skill learning and cortical circuitry

Abbreviated title: Developmental plasticity in the mouse motor system

Taehyeon Kim[1] and Bryan M. Hooks[1]

[1]Center for Neuroscience University of Pittsburgh (CNUP) and Department of Neurobiology, University of Pittsburgh School of Medicine, Pittsburgh, PA

Correspondence: Dr. Bryan M. Hooks, 200 Lothrop Street BSTWR Suite W1458 Pittsburgh, PA 15213; 412-624-8465; hooksm@pitt.edu (B.M.H.) and TAK127@pitt.edu (T.K.)

Number of pages: 42

Number of figures: 7 (5 Supplementary Data figures)

Number of tables: 0

Words for abstract (196), significance (132), introduction (890), and discussion (2374)

Conflict of interest statement: The authors declare no competing financial interests.

Acknowledgements: We thank Quincy Erickson-Oberg for assistance with the beam break experiment, Tom Deakin for assistance with rotarod experiment, and Kyle Bannerman for assistance with the gait analysis. We thank Omar Gharbawie, Chinfei Chen, Ghanshyam Sinha, and other members of the Hooks lab for feedback on the manuscript. This work was supported by a NARSAD Young Investigator Award (BMH), NIH NINDS R01 NS103993 (BMH), a Whitehall Foundation award (BMH), and an American Heart Association Predoctoral Fellowship (TK).

Abstract

Learning motor skills requires plasticity in the primary motor cortex (M1), including changes in inhibitory circuitry. But how inhibitory synaptic connections change during skill acquisition and whether this varies over development is not fully understood. This study assesses the normal developmental trajectory of motor learning and then addresses inhibitory connectivity changes after motor learning. We trained mice of both sexes to run on a custom accelerating rotarod at ages from postnatal day (P) 20 to P120, tracking paw position and quantifying time to fall and changes in gait pattern. Performance improved most rapidly between P30-60, while paw position and gait patterns change with learning, though differently between age groups. To address circuit changes, we labeled task-active and task-inactive pyramidal cells with CaMPARI2, a genetically encoded activity marker. We then evoked inhibitory responses (IPSCs) from two major interneuron types: parvalbumin-expressing (PV+) interneurons and somatostatin-expressing (SOM+) interneurons. After one training day, PV-mediated inhibition is greater in task-active cells, while SOM-mediated inhibition is not different. These results suggest early changes in PV-mediated inhibition may support motor skill acquisition in mice. Whether PV-mediated inhibitory changes persist or changes in SOM+ interneuron connections arise later in training remains to be tested.

Highlights

*Motor learning aptitude is developmentally regulated, peaking at P30-P45 for the cortically-dependent accelerating rotarod task

*Mice learn by shifting from hopping to walking gait, with the gait shift in forelimbs preceding the shift in hindlimbs

*Inhibitory responses in task-active neurons are stronger than task-inactive neurons from parvalbumin-expressing fast-spiking neurons on the first training day

*Other interneuron connections from somatostatin-expressing interneurons are unchanged

Significance Statement

Plasticity in sensory cortex is restricted to a limited developmental window. Learning motor skills requires motor cortex plasticity, but it is unknown whether there are changes in learning aptitude over development and whether the synaptic mechanisms of plasticity vary across cortical areas. Here, we define the developmental trajectory of motor learning aptitude for the accelerating rotarod task in mice. We find that learning peaks at P30-P45, with mice learning to shift from hopping to walking gait to stay on the rotarod longer. Further, the gait shift in forelimbs precedes hindlimbs. We then find, using recordings targeted to task-active neurons, that inhibitory responses from specific subtypes of interneurons (parvalbumin-expressing) are stronger in active cells, while other interneuron connections (somatostatin-expressing) are unchanged. These results suggest early changes in PV-mediated inhibition support motor skill acquisition.

Introduction

The critical period is a time during early development when neural circuits exhibit heightened plasticity in response to sensory experience[1–4]. The same sensory experience after the critical period does not cause the same magnitude of changes in the circuitry. Sensory areas have been extensively studied to define the critical period and its underlying circuit mechanisms. In both the visual and somatosensory systems, critical period timing is defined by deprivation of the corresponding sensation, such as incoming visual or whisker stimuli, and the resulting effects in the nervous system.

Plasticity in primary motor cortex (M1) is vital for the learning and executing of complex motor skills[5–7]. Studies of cortical plasticity have generally investigated sensory critical period plasticity, where manipulations at defined early ages can cause long-lasting changes in cortical connectivity and responsiveness, while plasticity is reduced or absent at later ages[8–10]. For visual areas, for example, critical period plasticity is limited to ~P18-P28 in mice[2,4,9]. Fewer studies have characterized plasticity during the corresponding period in M1 using motor skill acquisition. Most motor skill acquisition studies use young adults >1 month old. Motor skill acquisition across developmental ages in younger animals, closer to ages equivalent to the sensory critical period, is less unexplored. However, this requires addressing learning in a task that is cortex-dependent as well as one that animals of all ages can learn. Further, because skill acquisition can continue throughout life, it is worth exploring the degree to which plasticity is altered in later ages. Investigating age-related changes in motor learning will determine whether a period of heightened plasticity for motor learning exists, and how circuits mediate motor learning.

Voluntary movements and motor skill acquisition involves activity of subset of cortical cells, forming local circuit ensembles that may contain from 10-50% of local neurons depending on the task[11–14]. Motor skill acquisition is associated with structural and functional changes in these specific ensembles of excitatory neurons[13,15,16]. Neurons not related to the task may not undergo the same changes in connectivity and excitability. Because excitatory cells are the vast majority of cortical cells, much prior work, especially before transgenic approaches, has focused on local and long-range excitatory connectivity. M1 shares a number of local connectivity rules with S1 and other

sensory cortical areas[17–19], making a comparison to sensory plasticity of interest, especially as regards plasticity mechanisms. Prior work has suggested changes in the strength of corticocortical connectivity, potentially restricted to the upper cortical layers during motor learning[20–22]. This includes reweighting of long-range corticocortical and corticothalamic inputs[22]. Thus, plasticity in upper layers is likely to be involved in motor learning.

Cortical inhibitory circuitry is crucial for regulating plasticity. Inhibitory neurons are key circuit nodes in triggering in cortical plasticity in sensory areas. The opening of the critical period is caused in part by the maturation of GABAergic inhibition[2]. Further, transplantation of the inhibitory neurons can induce a period of heightened plasticity later in life[23,24]. Similarly, in motor areas, inhibition also regulates plasticity. Reduced inhibition is inversely correlated with motor learning performance in normal and post-injury conditions in humans and mice[25–30]. Still, the mechanisms governing plasticity for motor learning are not fully known. Many, but not all, features of circuit connectivity and plasticity are conserved across cortical areas. About 30% of cortical neurons are inhibitory interneurons[31,32]. Subtypes of inhibitory neurons can be further categorized based on molecular markers, electrophysiological characteristics and morphology[31,32]. Two major inhibitory interneuron types are parvalbumin-expressing (PV+) and somatostatin-expressing (SOM+) interneurons [31]. PV+ and SOM+ interneurons connect in the circuit differently. PV+ interneurons inhibit excitatory neurons, synapsing near the soma, while SOM+ interneurons synapse on distal dendrites of excitatory cells[33–35]. PV+ inhibition can be reweighted rapidly in an activity-dependent manner, providing greater inhibition to more active pyramidal cells[36,37].

How does the role of interneuron plasticity in sensory critical periods compare to that in M1? It is not as straightforward to fully deprive M1 of activity, though it has been attempted[38,39]. Thus, we chose skill acquisition to observe changes during development. Similar to excitatory neurons, inhibitory neurons go through both structural and functional changes. SOM+ interneurons show a temporal shift in their activity with learning[40]. PV+ interneurons in particular have a transient increase in activity in motor cortex and retrosplenial cortex[41]. Due to their axodendritic targeting[34,35], SOM+

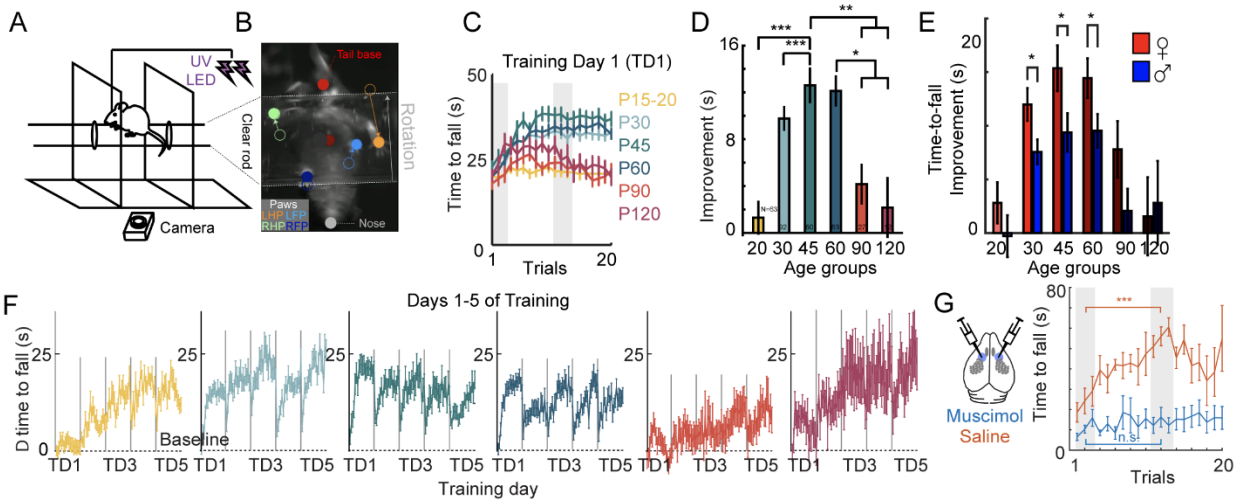

Figure 1 | Rotarod skill acquisition plateaus around P30-P60 on training day 1.
(A) Schematic of rotarod task with high speed videography and barriers to create the running lane during a trial. (B) Video frame of mouse during running. Paw positions (LFP, left front paw; LHP, left hind paw; RFP, right front paw; RHP, right hind paw) and the nose and tail base are tracked using DeepLabCut. (C) Learning curve during 20 trials on training day 1 (TD1). Six colors represent the six ages tested (P15-20, P30, P45, P60, P90, and P120). Gray bars represent time windows used for early and late performance to assess TD1 improvement. (D) Improvement (in seconds) in time to fall during TD1 for six age groups. Mean+/- SEM. N=63, 92, 60 63, 27, 12 . (E) Improvement (in seconds) in time to fall during TD1 for six age groups, subdivided by male (blue) and female (red). Mean+/- SEM.(F) Improvement (in seconds) in time to fall during five training days. Gray vertical lines divide the days. Mean+/- SEM. (G) The effect of M1 inactivation by bilateral muscimol injection on rotarod skill acquisition compared to saline injected controls. N=5 (control); N=9 (muscimol). Mean+/- SEM. Significance: *, p<0.05; **, p<0.01; ***, p<0.001.

interneurons are well-situated to mediate the changes in dendritic spines with motor learning. Transient silencing of SOM+ cells leading impairment in motor learning further implicate SOM+ cells' role in skill acquisition[1,40], but exact synaptic changes, including synaptic strength, are unclear. Learning a lever pressing task, another type of motor learning paradigm, induces structural changes in axonal boutons of both PV+ and SOM+ populations[1]. While PV+ axonal boutons transiently increased, SOM axonal boutons decreased, but more slowly over several days of learning[1]. Similar interneuron-dependent changes likely occur in M1 during rotarod training. It is unknown whether the postsynaptic targets of these axons that undergo dynamic changes are task-related cells. The experiments here test whether changes in cortical inhibition regulate M1 plasticity. Below, we directly test whether the observed structural changes in axonal boutons lead to functional changes of inhibitory synapses by defining ages with peak plasticity and addressing whether changes in interneuron-mediated inhibition strength occurs during motor learning.

Results

Rotarod performance peaks and plateaus around P30-60.

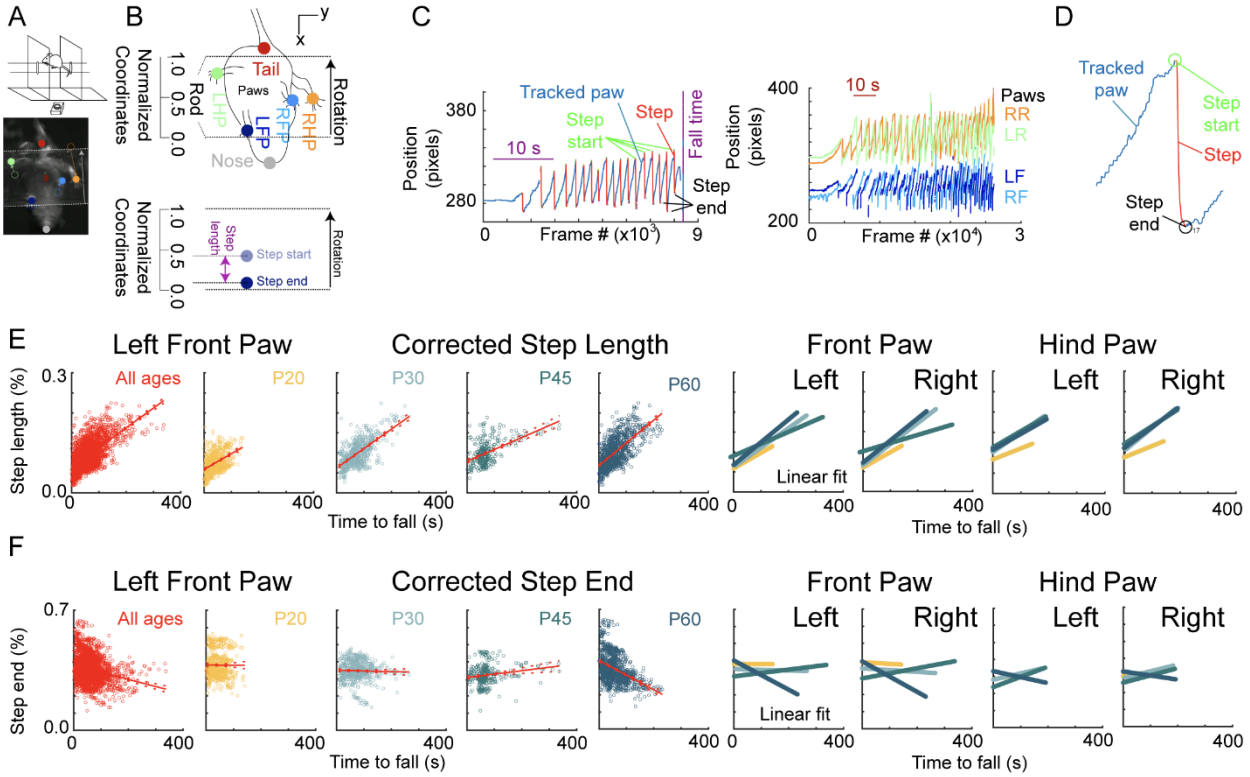

Figure 2 | Tracking step kinematics during rotarod training.
(A) Schematic of rotarod task with video frame of tracked mouse. (B) Cartoon of tracked image frame illustrating location of the mouse paws (LFP, left front paw; LHP, left hind paw; RFP, right front paw; RHP, right hind paw) and the nose and tail base using DeepLabCut. The rotarod and direction of motion are indicated, with the front and rear ends of the rod serving as 0.0 and 1.0 in normalized coordinates. At bottom, coordinates for the step start, step end, and step length are plotted to illustrate how they are determined. (C) Plot of the x-position of a single paw (LHP, left) or all paws (right) during a trial. Time given in frames (converted to seconds with example timebar). (D) Expansion of paw tracker showing step detection. Steps (red) are automatically detected (see methods). Step start (green), step end (black), and step length are then calculated. (E) Step length versus time to fall for the left front paw, plotted for all ages combined (red) and individual ages (20 and above). Data are fit to a line and the linear fit compared at right. Summary plots include step length versus time to fall for the right front paw, left hind paw, and right hind paw (far right). (F) Step end point presented similarly to step length.

Mice become ambulatory by P15. Walking is part of natural locomotion that can be tracked in mice at a range of ages and sizes. To test motor learning, we used the accelerating rotarod task, which takes advantage of walking on an accelerating rod. Furthermore, improvement in the task can be observed within a single training day. The time to fall and changes in foot position were measured to determine the learning curve at different ages. To monitor changes in the gait, we built a custom rotarod made of clear plexiglass and a high-speed camera was mounted at the bottom to record the behavior (Figure S1A-B). Six age groups were used to test the age-related differences in the aptitude to learn a motor task: P15-20, P30, P45, P60, P90 and P120 (Figure 1A-D). Typical behavior during the first training day for these ages tended to improve during the first half and reach a plateau within the first session, with some reduction in performance in later training day 1 trials. We wanted to measure the improvement by

comparing the time to fall when the animal was at beginner level (early phase of learning) and when the animal reached an expert level (when they reached plateau). Thus, improvement was calculated by subtracting the average time to fall measured in trials 11-13 (when the performance tends to reach plateau) from the average time to fall measured in trials 1-3 (beginner; Figure 1B-D). Within the first two months of age, the improvement was greater for the animals in P30-60 compared to those in the P15-20 group (Figure 1D, $p<0.001$). Compared to P90-120 animals, the animals in P45-60 showed significantly greater improvement (Figure 1D, $p<0.01$ (P45) and $p<0.05$ (P60)).

Testing a behavioral task across different age groups came with some confounds. Although this task used no external rewards to exploit the natural walking behavior in mice, it was possible that age-dependent differences in the time spent walking in the home cage might contribute to rotarod performance. To assess if there was a difference in baseline locomotion, animals were tracked in a standard cage with infrared beam breaks to determine the number of times they crossed the length of the cage. P15 mice crossed the least number of beam breaks compared to the other age groups (Figure S2, $p<0.001$). P45 animals exhibited a greater number of beam breaks compared to P30 (Figure S2A, $p<0.001$), but there were no other significant differences within these older ages.

We next considered sex as a variable. Significant sex differences in improvement were observed in the P30, P45, and P60 groups (Figure S3, $p<0.05$), with young adult female mice outperforming males in these age groups. Because adult male mice tend to weigh more than female mice, we considered that the sex difference in performance might be due to weight. From P20 to P120, each age groups gained significant weight (Figure S2C). Male mice significantly outweighed female mice at ages above P30 (Figure S2D). Across all ages, there was no correlation between weight and improvement, nor was there a correlation in a specific sex (Figure S2E). P60 had a significant correlation between improvement and weight ($p=0.0496$). However, no particular age group showed sex-specific correlation with performance. Therefore, weight alone did not explain differences in performance, since there were not significant differences between heavier and lighter mice at P30-P60.

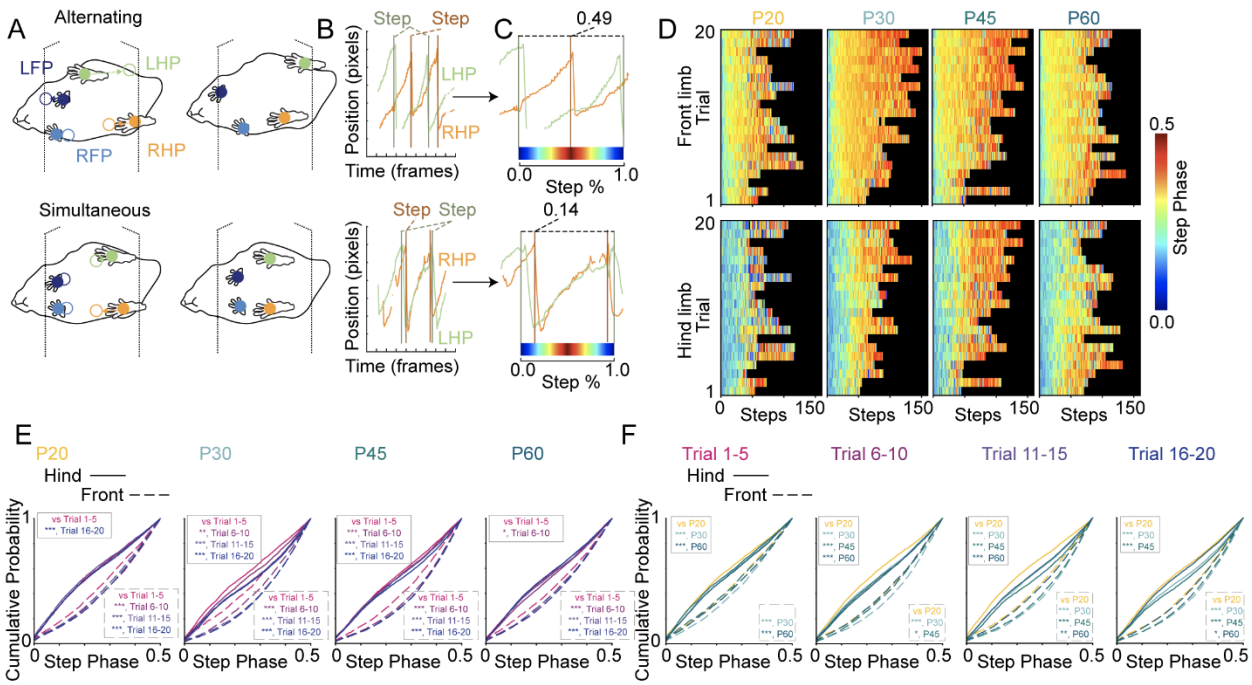

Figure 3 | Gait pattern changes with age and training.
(A) Schematic of rotarod task with video frame of tracked mouse. (B) Cartoon of tracked image frame illustrating location of the mouse paws (LFP, left front paw; LHP, left hind paw; RFP, right front paw; RHP, right hind paw) and the nose and tail base using DeepLabCut. The rotarod and direction of motion are indicated, with the front and rear ends of the rod serving as 0.0 and 1.0 in normalized coordinates. At bottom, coordinates for the step start, step end, and step length are plotted to illustrate how they are determined. (C) Plot of the x-position of a single paw (LHP, left) or all paws (right) during a trial. Time given in frames (converted to seconds with example timebar). (D) Expansion of paw tracker showing step detection. Steps (red) are automatically detected (see methods). Step start (green), step end (black), and step length are then calculated. (E) Step length versus time to fall for the left front paw, plotted for all ages combined (red) and individual ages (20 and above). Data are fit to a line and the linear fit compared at right. Summary plots include step length versus time to fall for the right front paw, left hind paw, and right hind paw (far right). (F) Step end point presented similarly to step length. Significance: *, $p<0.05$; **, $p<0.01$; ***, $p<0.001$.

To determine whether learning on the accelerating rotarod is M1-dependent task, M1 was pharmacologically inactivated by bilaterally injecting muscimol in P30-45 animals. Mice that received either muscimol or saline bilateral injections were permitted to recover from the procedure for 40 minutes and showed normal ambulation in the home cage after recovery. When tested on the accelerating rotarod, muscimol-injected animals did not show improvement compared to the saline-injected littermates, confirming that the task is an M1-dependent task (Figure 1G).

Changes in paw kinematics are correlated with better performance

Although time to fall was an effective measure of overall task performance, a more detailed understanding of how animals improved during the task was achieved by high-speed videography to quantify changes in limb movements. This approach tracked limb kinematics by acquiring video of paw position through the clear rod. During rotarod training, four paws, the nose, and the base of the tail were tracked with DeepLabCut

(Figure 2A-B). Estimated positions of these parts were tracked in x- and y-coordinates in the video, with the x-axis aligned to the direction of rod rotation. Paw positions were filtered by likelihood (>0.95) and steps were automatically detected based on the prominence of the peak in the trajectory with a minimum interstep interval using custom software in Matlab. Step end and step start positions thus extracted were then normalized to the width of the rod (Figure 2B). Step length was the normalized distance between the step end and the start (Figure 2B). Raw position in pixels was plotted to demonstrate accuracy of the step detection, while the paw position for all paws can be simultaneously tracked (Figure 2C-D).

We then examined how paw kinematics changed during learning by comparing the normalized step length and step end point with performance (Figure 2E-F and Figure S4), measured as time to fall. When pooling data across ages, a few general trends emerged. First, longer step length was associated with longer times on the rotarod. This was consistent across all ages measured (P20-P60). The increase in step length was similar for both front and hind paws. Second, the step end point moved closer to the front edge of the rotarod. This effect was strongest for front paws but was present to a lesser degree for hind paws (as expected if step size also increases). This effect, however, varied with developmental age, being present and pronounced in P60 animals, shifting the location of the front paw to end steps from about 0.4 (closer to the middle) to about 0.2 (close to the edge of the rod). At other ages, the step end position is static.

Changes in gait patterns are correlated with better performance

The rotarod task involves not only kinematic changes in individual paws, but also the coordination of left and right paws. Animals engaged in different types of gait patterns during the task – simultaneously moving both paws (hopping; Figure 3A) or alternating the left and right paws (walking; Figure 3A). To determine how the gait pattern changed, we needed to consider the phases of steps between left and right paws. We compared the step times of the paws and assigned each step a score (range 0.0 to 1.0). The step time of the left paw (Figure 3C, green for the left hind paw) was marked. The time between two left steps was normalized from 0.0 to 1.0. The time of

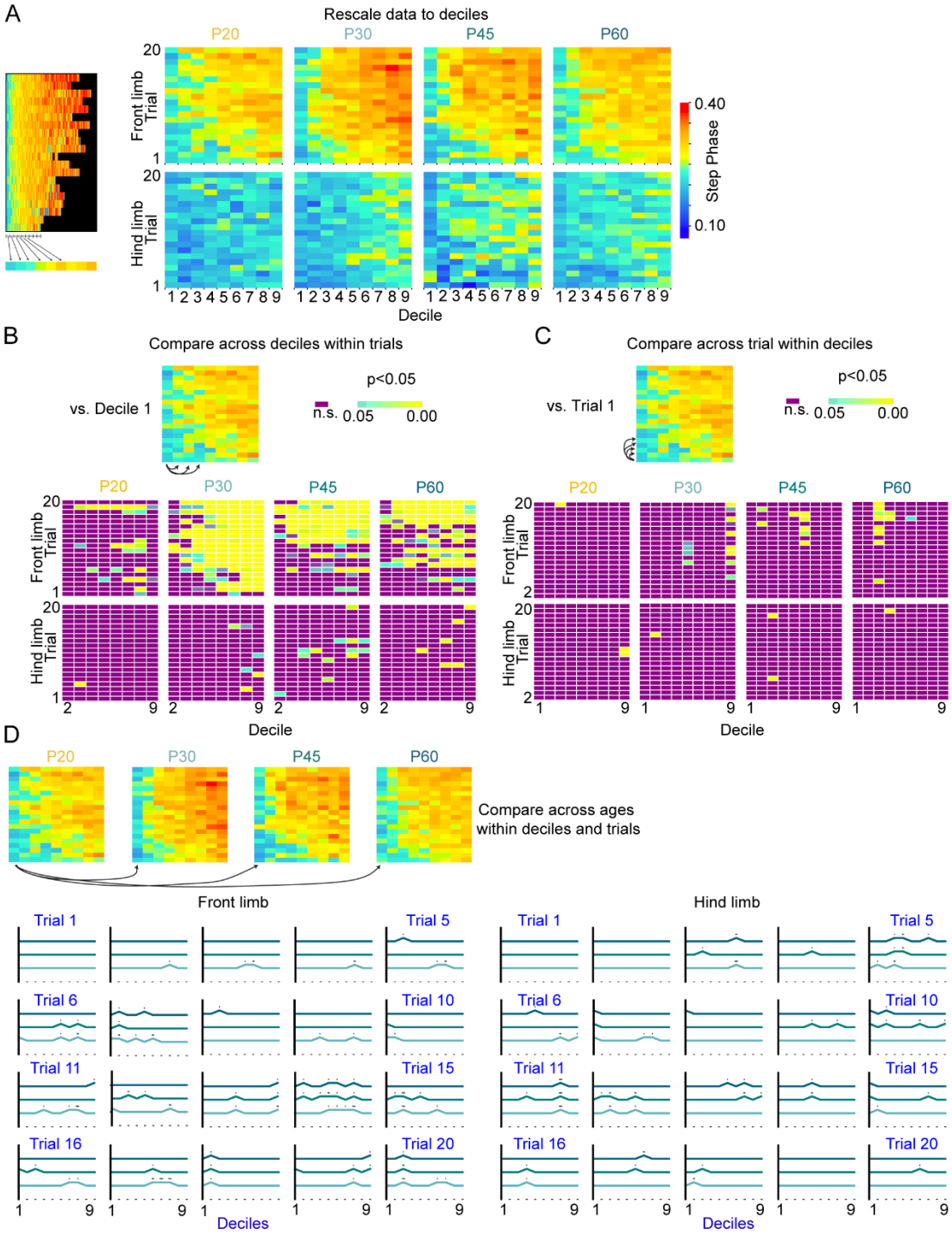

Figure 4 | P-values for the gait analysis.
(A) Due to variations in the number of steps, the number of steps in a trial were divided into deciles to facilitate the comparison of average step phases across trials and age groups. The average step phase value for each age for front and hind limbs is plotted. (B) The P-value plot of deciles compares the first decile of trials 1-20 to rest of the deciles (2-9) for each trial. The top row compares front paws at four ages and the bottom row compares hind paws. Non-significant p-values are purple; p-values < 0.05 are as shown in the lookup table. (C) The P-value plot comparing across trials compares each decile from trials 2-20 with the corresponding decile from trial 1. The top row compares front paws at four ages and the bottom row compares hind paws. For instance, the front paw in P20 Decile 3 from trial 3 is compared to Decile 3 from trial 1. Non-significant p-values are purple; p-values < 0.05 are as shown in the lookup table. (D) The P-value plot of deciles compared across ages assess P20 versus P30, P45, and P60 groups for 20 trials. Each individual graph represents the comparison between the four age groups for a given trial. The X-axis denotes deciles, with a specific trial's decile being compared to the corresponding decile of the P20 group. For example, the front paw in P30 Decile 9 is compared to P20 Decile 9 in the trial 1 graph, and if significantly different, it is indicated by a bump in the y-axis.Significance: *; p<0.05. **;p<0.01, ***;p<0.001.

the right hind paw step (orange) was then computed as a fraction of the relative

distance between left steps. Alternating gait occurred when phase difference of the left and right paws was closer to 0.5 while the simultaneous or hopping gait was closer to 0.0 or 1.0 (Figure 3C). Note the color map at the bottom that signifies the alternating gait as red and the hopping gait as blue. The scale was reflected because we treated step phase scores from 0.5 to 1.0 as equivalent to 0.5 to 0.0 to assess alternating gait. To determine changes in gait pattern on the first training day and how these differed with limb, age, and trial number, the data were plotted as follows. For each step taken, such as the first step on the first trial (of 20), the mean step phase score was computed across all mice tracked, and the corresponding color plotted as a tick mark (Figure 3D). These were generally blue (simultaneous/hopping gait). This was repeated for each subsequent step and for each trial. The number of steps included in the average varied across the row for each trial, reflecting the variability in performance (as observed in time to fall) within and across trials. Qualitatively, both front limb and hind limb and within each age, the gait pattern generally shifts from hopping to walking (alternating gait). This shift seemed to occur more rapidly for the front paws than the hind paws, suggesting that the transition to a walking gait can occur at different time for the two pairs of limbs.

To determine whether the gait pattern shifted significantly on the first training day, the cumulative frequencies of the step phases at four different stages of the training were plotted (Figure 3E): beginner (trials 1-5), early learning (trials 6-10), mid-learning (trials 11-15), and late learning (trials 16-20). The offset in step phase between front limbs (dotted lines, lower right) and hind limbs (solid line, upper left) was evident in the data, suggesting that the front and hindlimbs employ different strategies during rotarod training. Cumulative frequencies of the phases in beginner stage were compared to the other three stages. Across all age groups, the front paws shifted to alternating gait starting from early learning at all ages (trials 6-10) (Figure 3E, left). On the contrary, the shift from simultaneous hopping to alternating in the hind paws was delayed in the P20 group (Figure 3E, left). While animals in P30-60 groups transitioned to alternating by early learning (trial 6-10), P20 groups did not start alternating until late learning (trials 16-20).

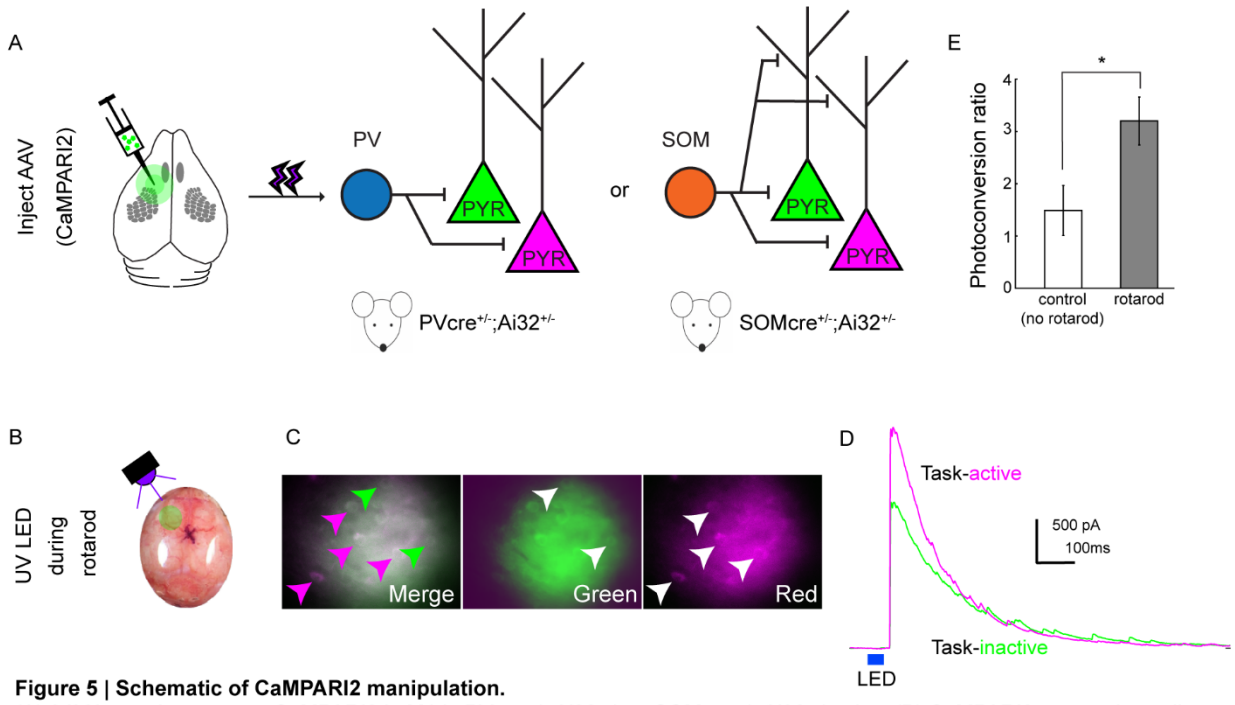

Figure 5 | Schematic of CaMPARI2 manipulation.
(A) AAV is used to express CaMPARI2 in M1 in PVcre+/-;Ai32+/- or SOMcre+/-;Ai32+/- mice. (B) CaMPARI2-expressing cells are photoconverted to red by a skull-mounted UV LED. (C) Example images of a slice after photoconversion during rotarod. (E) Example traces from GFP+(green) and RFP+ (red) neurons after optogenetic stimulation of PV+ cells. (F) The photoconversion ratio is calculated by dividing red fluorescence by green fluorescence. Animals showed a greater photoconversion ratio after the rotarod task (grey) than the control animals that freely moved in the chamber (white). Significance: *; p<0.05.

However, the change in the distribution of the gait patterns over time within a trial were not well-quantified in this manner. We wanted to compare whether there was a difference in the emergence of a gait pattern and compare between age groups and trials. To do so, the entire length of the steps in a trial were averaged into deciles which were then compared between deciles, trials and age groups (Figure 4A). This appeared similar to the raw data (Figure 3D), with all trials now scaled to the same length. This approach allowed us to look at the changes in gait pattern despite the difference in the number of steps in each trial. First, to compare whether gait pattern evolved within a trial, we compared the first decile of a given trial to the rest of the deciles in the same trial. This showed the strongest effect: The phase of the front paws, particularly in P30-60 groups, showed significant differences compared to the first deciles across many trials (Figure 4B). P30 groups showed most difference in the phase of the front paw compared to the first decile. Hindpaws seemed to show few significant differences across deciles. P30 and P60 showed some difference in late deciles while P45 showed a few early-mid late deciles difference along with later decile differences in mid learning.

P20 group showed minimal difference in phase of hind paws. Second, to test whether there was a difference in gait across trials, the decile of the first trial was compared to the corresponding decile of the rest of the trials (trial 2-20). This effect was considerably weaker (fewer significant comparisons). In the P20 group, both front and hind paws showed little difference across trials (Figure 4C). In the P30 group, the difference in front paw occurred early-mid learning (as early as trial 5) in late deciles (Figure 4C). In the P45 group, the difference in the front paw appeared later and became more evident around mid-learning, particularly in early-mid deciles. In the P60 group, differences in front paw started to predominantly appear in late trials on the first training day (Figure 4C). As before, the difference in hind paw gait across the age groups was minimal and inconsistent (Figure 4C). Lastly, to compare between age groups, we compared a decile in a given trial of P20 to a corresponding decile in the same trial of P30, P45 or P60 (Figure 4D). Front paws of P30 started to show differences in early trials and differed from P20 throughout many of the trials (Figure 4D). On the other hand, P45 and P60 showed difference to P20 later trials (Figure 4D). Trial 14 seemed to show very different gait pattern in P30-60 compared to P20(Figure 4D). Hind paws P30-60 showed differences compared to P20 as early as Trial 3 during early learning and this persisted throughout many trials (Figure 4D).

PV+ interneurons provide greater inhibition to task-active cells following one training day

When the cells are active during rotarod performance, CaMPARI2 is photoconverted from green to red fluorescence following UV-light delivery, while the CaMPARI2 in inactive cells remains green (Figure 5A-D)[42]. To ensure that photoconversion was specific to activity during the rotarod task, we performed a control experiment. Animals aged from P20-60 received UV-light while freely moving at the bottom of the behavior chamber under the rotarod to simulate the same environment without motor learning. The duration for which the animals stayed in the chamber was determined by the average time to fall in training day 1 for the age- and sex-matched group. Photoconversion (red/green) ratio was significantly less than those measured from animals that completed the rotarod task (Figure 5F). To assess changes in

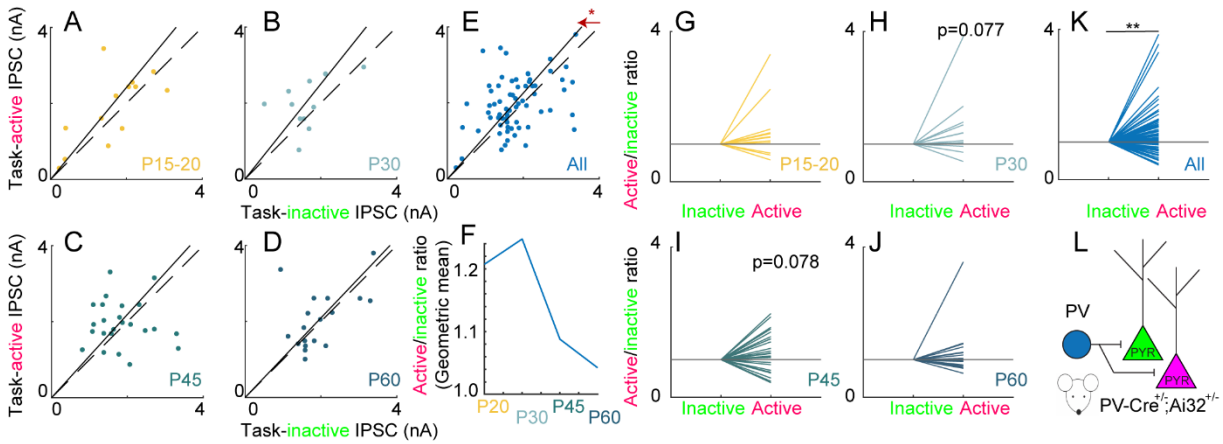

Figure 6 I IPSCs recorded in task-active (RFP+) vs. task-inactive cells (GFP+) after stimulating PV+ interneurons
(A-E) Scatter plot of IPSC responses in pairs of task-active (red) and task-inactive (green) cells in P20 (A), P30 (B), P45 (C), P60(D) and across all age groups (E). Solid line is the geometric mean of the pair responses. Dotted line is the line of equality (x=y). (F) Slopes of geometric mean across all ages plotted together. (G-K) Ratio of responses of task-active cells to their partner task-inactive cells after PV+ stimulation in P20 (G), P30 (H), P45 (I), P60 (J) and across all age groups (K). Significance: *, p<0.05; **, p<0.01; ***, p<0.001. (Also indicated with red arrows in (A-E). (L) Schematic of the genetic strategy for testing PV output to M1 pyramidal neurons.

inhibitory synaptic connectivity, we made whole-cell recordings in M1 layer 5 excitatory neurons that were either red or green to determine whether the inhibition provided by either PV+ or SOM+ interneurons differs in an activity-dependent manner. Inhibitory responses (IPSCs) were optogenetically evoked in either PV+ or SOM+ neurons to measure synaptic strength (Figure 5E).

Figures 6 and 7 show the scatter plot of peak IPSC recorded in pairs of task-active (red) and task-inactive (green) cells (same slice) after evoking either PV+ or SOM+ interneurons in animals. The dotted line on the plot is unity line where the responses of task-active and -inactive cells would be equal, and the slope of the solid line is a geometric mean. Across all ages, the geometric mean of the pair responses lied left of a line of equality for PV+ stimulation groups (Figure 6). Thus, a shift to the left of the dotted line represents input favoring task-active neurons, while a shift to the right favors task-inactive neurons. Across all ages, PV-mediated inhibition was greater in red (task-active) than those in green (task-inactive) neurons (Figure 6E, $p<0.05$). Furthermore, responses recorded in RFP+ cells were normalized to their partner GFP+ cells (Figure 6G-K and 7G-K). After normalization, PV-mediated inhibition in red (task-active) neurons was greater than those in green (task-inactive) neurons in all ages combined (Figure K, $p<0.01$). P30 and P45 groups showed a trend in greater inhibition on red (task-active) compared to green (task-inactive) cells (Figure 6H and I). On the contrary, when SOM+ cells were optogenetically stimulated, IPSCs recorded in red

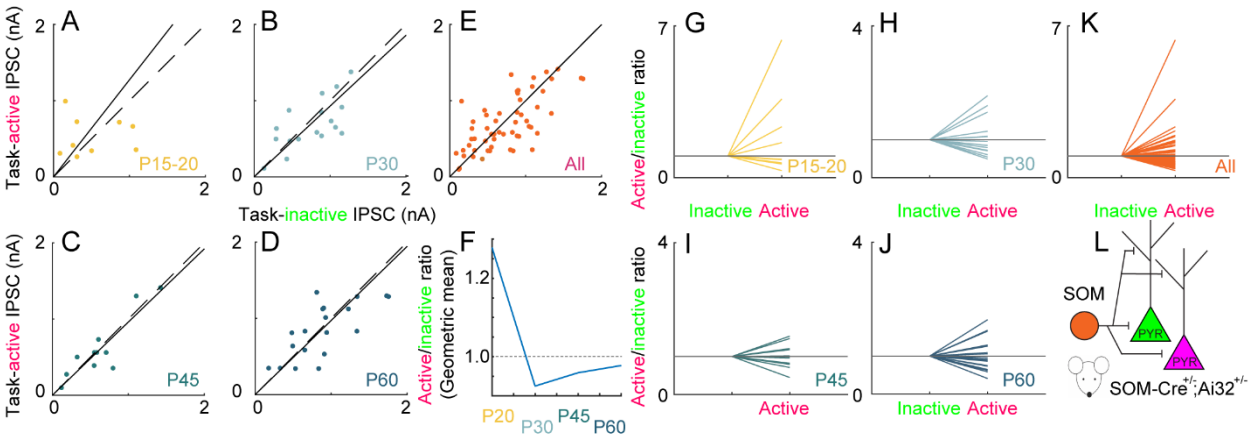

Figure 7 I IPSCs recorded in task-active (RFP+) vs. task-inactive cells (GFP+) after stimulating SOM+ interneurons
(A-E) Scatter plot of IPSC responses in pairs of task-active (red) and task-inactive (green) cells in P20 (A), P30 (B), P45 (C), P60(D) and across all age groups (E). Solid line is the geometric mean of the pair responses. Dotted line is the line of equality (x=y). (F) Schematic of the genetic strategy for testing SOM output to M1 pyramidal neurons. (G-K) Ratio of responses of task-active cells to their partner task-inactive cells after SOM+ stimulation in P20 (G), P30 (H), P45 (I), P60 (J) and across all age groups (K).

(task-active) cells were not significantly different from those recorded in green (task-inactive) cells (Figure 7G-K). Thus, our data suggest that motor learning induced cell-type-specific changes in inhibition depend on the activity of the postsynaptic target on the first training day, but only for PV+ and not SOM+ interneuron connections.

Discussion

Rotarod Motor Skill Learning is Fastest in a Given Developmental Window

To address age-dependent differences in motor learning, we first used a walking task that was consistent with the range of natural behaviors in mice. Walking is a common behavior in vertebrates that relies, in part, on central pattern generators in the spinal cord[43]. For mice, walking begins naturally prior to the ages we test. To assess whether there is a sensitive (critical) period in the ability to acquire a motor skill, we tested mice as young as P15 (who could still execute the task) up to age P120 on the accelerating rotarod. Using time to fall as a measure of learning, these data show that first day improvement in performance on the rotarod varies with age, plateauing at P30-60. This suggests that there are differences in the aptitude for motor learning across developmental time. This is unlikely to be due to difference in the baseline locomotion, which does not show a heightened activity selectively at P30-60 (Figure S2A-B). Previous experiments had also shown that prior exposure to exercise did not affect

learning[44]. Control experiments also ruled out effects of weight within each age cohort (Figure S2E). Since improvement does occur over five days of training for all age groups of mice (Figure 1F), the animals are physically capable of executing the task at all ages. Although using a skilled reaching task to explore age-dependent differences in skill learning is possible, it was not as clear that P15-P20 mice could execute this task.

The rotarod task was unrewarded, as mice walk naturally and running is an intrinsically motivated behavior[45,46]. This removes the confound of reward circuitry with motor learning. Although all ages learn, and some learn faster, it is not clear whether other aspects of the animal's motivational state might differ across age and contribute to task performance. If low motivation accounted for poor TD1 performance in P20, P90, and P120, this does not explain how motivation changes on subsequent days of training as behavior improves, while potentially differently motivated P30, P45, and P60 mice do not have large swings in motivation. It is possible that instead of motivation, differences in anxiety contribute to performance differences at different ages. An assay for fear might clarify this, though a nonlinear age-dependent variation in fear would be interesting to explore in other circuits.

It is difficult to assess whether learning is a shift in mindset where the animal understands the goal of the task (walk so as to stay on the rod), or whether the goal is clear and learning is a shift in precision of skilled movement. Both shifts could result in a successful increase in time to fall. Although these experiments do not clearly distinguish between these alternatives, tracking the kinematics of paw movement suggests that, at least in part, better performance is associated with changes in motor control. This seems to be the case because the step lengths for all paws evolve during the task (Figure 2E), front paw step end points are targeted closer to the end of the rod, at least for P60 (Figure 2F), and gait pattern evolves with time during the task (Figure 3 and 4B). Differences in sex did account for differences in performance, with female mice performing better during P30-P60 (also corresponding to the peak period of learning-related plasticity). Beyond ruling out weight as a factor, the basis for improved female performance during this time window was not explored further, though there is evidence of mechanism differences in other systems[47] that invite future efforts to probe M1 circuitry in a similar way.

Because spinal circuits also play a role in control of walking, it is important to test whether rotarod skill learning depends on motor cortex. This task has been used in previous studies of motor cortex to assess circuit changes during learning. Specifically, rates of spine formation and retention in forelimb M1 change during rotarod learning[15,16]. Not only are there structural changes, but the firing patterns of neural ensembles show task-specific modulation during training and reorganize over several sessions to support motor learning task[11]. Together these imply that circuit changes assist in acquiring a new skill. Consistent with this, our data shows that bilateral inhibition of forelimb M1 with muscimol during rotarod training blocks motor learning relative to saline injected control mice (Figure 1G). Normal walking (in the home cage), however, was not affected and these mice exhibited other non-learned forelimb behaviors, such as jumping. Collectively, this suggests a necessary role for forelimb M1 in rotarod learning.

Transition from hopping to walking gait facilitates motor learning best in P30-P60 mice

Markerless tracking[48] enabled tracking paw position and segmenting paw trajectories into steps (Figure 2). This was essential to understanding changes in paw kinematics as well as comparing steps to understand gait changes. Step length was tracked for all four paws and showed a consistent effect across age groups. For both forepaw and hindpaw, steps became longer as mice were more successful at remaining on the rotarod. Further, while the trend was similar, P20 mice took shorter steps compared to the other age groups, consistent with smaller body size. Targeting of step endpoint relative to the end of the rod was more complex. In general, the endpoint location was relatively stable during learning across ages, with the exception of the P60 mice. P60 animals developed a strategy of placing the forelimb step closer to the front edge of the rotarod. The effect was smaller but present for the hind limb because the step length became longer. This suggested that mice were able to change some of the kinematic parameters of their steps, including targeting a specific location on the rod. Whether this step location targeting requires somatosensory[49] or visual feedback is not clear, although the experiments were run in the dark with infrared light.

More interesting than step kinematics is gait pattern. Overall, gait shifts from hopping to walking as individual trials proceed. But the shift is more pronounced for certain trials and at certain ages. Further, the shift from hopping to walking appears to happen at different times for forelimbs and hindlimbs, suggesting that the circuitry controlling the mode of locomotion can operate independently for each pair of limbs. The shift from hopping to walking strategy enables animals to stay on the rod, though it is unclear whether a split in gait pattern between forelimb and hindlimb would occur in other more naturalistic conditions. Notably, humans are able to walk at different speeds between the left and right leg on a split treadmill[50], but interpreting this adaption is difficult. That the targeting of the paws closer to the front edge of the rod and the change in gait occur in a more pronounced way for the forelimb suggests that the motor learning may involve this limb more than the hindlimb. If the learning were simply a response to movement of the rod, sensory feedback and balance, this might be more likely to involve both limbs, while specific involvement of the forelimbs might imply a more a deliberative or conscious effort that involves frontal cortex.

What about differences in the gait shift? These data can be compared across bins within the same trial, for the same bin across trials, and across ages. Within the first training session, forelimb step phase shifts significantly towards walking for ages after trial 5 (Figure 3E). However, the shift for hindlimbs in the same comparisons is strongest only for P30 and P45 (Figure 3E). This suggests that forelimb performance is more plastic in this assay, and that the hindlimb plasticity is also enhanced at certain ages (P30 and P45). When comparing across ages at the same trial number, older animals perform better than P20 animals for all ages compared (Figure 3F). This shift appears larger and has more statistical support for later trials (Figure 3F, Trials 11-15 and Trials 16-20). These plots, however, do not account perfectly for shifts in gait since they compare steps across the entire trial (but see Figure 4D). Subdividing the steps into bins by fraction of steps taken on a given trial, a more detailed comparison with fewer steps per bin can be made, though this reduced the statistical power. In this approach, the strongest effects were observed across deciles in a given trial for the front limbs, further supporting the plasticity of the front limb.

Cell type specific changes in cortical inhibition for task-active networks

Previous reports demonstrated that motor learning was accompanied with reduction in inhibition. In our experiments, PV+ cells provide greater inhibition to the active cells while SOM+ cells provide similar amount of inhibition. The discrepancy could arise from our approach and experimental design that not only distinguishes the interneuron subtype but also its postsynaptic target by their activity during learning. We directly probed the changes in inhibition mediated by PV+ and SOM+ interneurons to the pyramidal cells depending on their task involvement.

Similar to our observation, learning a lever pressing task, another form of motor learning paradigm, induces transient increase in PV+ axonal boutons, their activity, and immunoreactivity of PV+ which positively correlate GABAergic activity[1,41,51]. This suggests that PV+ may regulate motor learning, particularly in early phases, by transient increases in its connection strength to excitatory neurons. This increased inhibition by PV+ could be a homeostatic mechanism to balance the increased activity in task-active pyramidal cells by increasing inhibition[36,37]. PV+, but not SOM+, interneurons modulate their inhibition depending on the relative activity of the post-synaptic pyramidal cell in V1 [36]. This homeostatic effect may be part of forming specialized subnetworks[52,53] to recruit M1 neurons in a specific spatiotemporal pattern that emerges with training[13,40,54]. In contrast to a homeostatic change, perhaps PV+ synaptic changes occur first and pyramidal neuron activity is altered following this change. Another possibility is that the PV+ interneurons may be involved in shift in the timing of pyramidal cell activity with motor learning. PV+ neurons affect the oscillation of pyramidal cells, particularly in the gamma band[55,56]. Gamma oscillation can be observed during cognitive tasks and recently with motor learning[57–59]. Timing of inhibition can modulate spike timing, potentially influencing the temporal shift in excitatory activity. During reaching task, the activity of PV+ interneurons precede the activity of putative excitatory neurons[60]. During the rotarod task, their timing of activity in relation to their post-synaptic excitatory partner may modulate the firing of excitatory cells in an activity-dependent manner. We observed a trend in increase in inhibition in P30-45 groups, but not in P20 and 60. This suggests that the circuit mechanisms of motor learning can vary with age in motor cortex. Even at postnatal ages, PV+ interneurons go through significant maturation in

both sensory and frontal areas[61–63]. Even though P60 animals are capable of achieving similar level of motor learning as P30-45 animals, the circuit changes that support learning may take a different form once the circuitry has matured after P60 and onward.

The synaptic changes in PV+ input are detectable on the first training day. It is unknown if the synaptic changes by PV+ neurons are persistent or transient (thus will be eliminated with further training as the task becomes consolidated). PV+ axonal bouton and activity changes, for example, are transient[1,41] and with enough training, inhibitory activity to perform the task and potential mechanism to refine the cortical circuit may no longer be needed and move out of cortex [5,64].

Even though our study did not observe difference in inhibition mediated by SOM+ interneurons, synaptic changes in these neurons may occur with a longer time course[1,41,65]. Additional factors that may explain our results. First, SOM+ interneuron postsynaptic targets include other inhibitory neurons, along with pyramidal cells[33]. Thus, changes in their activity could influence inhibition onto other inhibitory interneurons. A second potential factor is that due to their subcellular targeting on dendrites and our recordings done on soma, changes in SOM+ mediated inhibition on distal dendrites may not have been detected with our approach. Dendritic recordings might elucidate whether SOM+ inhibition also differs depending on the activity of the postsynaptic targets. A third potential explanation is that the changes in SOM+ cells may take longer to occur following learning. Unlike the changes in PV+ interneurons, changes in SOM+ cells are more persistent[1,41,66]. For future studies, it would be useful to follow SOM+ connectivity changes in later training days, while learning plateaus and animals reach expert level.

We targeted our recordings to task-active neurons in L5. This can be further divided into sublaminae: L5A (upper) and L5B (lower). These sublaminae contain different types of long-range projecting excitatory neurons: IntraTelencephalic (IT-) type neurons (whose projections target ipsi- and contralateral cortex and striatum) and Pyramidal Tract (PT-) type neurons (whose projects target ipsilateral subcortical structures, including striatum, thalamus, superior colliculus, brainstem, and spinal cord) [67]. IT- and PT-type neurons are the major output neurons of the motor cortex and are critical in the preparation and execution of a movement in the motor cortex[68–71]. Their involvement in preparation and execution of voluntary movement is different[68–72]. With

our current approach, however, we cannot distinguish between these two excitatory cell types while maintaining the task-involvement through CaMPARI2; thus, we cannot conclude if PV+ or SOM+ differentially inhibit these neurons in an activity-dependent manner.

Our study has demonstrated that the aptitude of animals to perform on an accelerating rotarod task differs depending on the age. Animals between P30-60 perform better than the younger age groups (P20) and older age groups (P90-120). In addition, learning is accompanied with changes in the paw kinematics and gait. Animals tend to take larger steps and shift the gait from hopping to walking, which is more pronounced and happens earlier in the trial in forelimbs. After a single training day, PV+, but not SOM+, induced greater inhibition in task-active postsynaptic cells than its neighboring task-inactive cells, suggesting a role of activity dependent PV+ inhibition during early learning. However, this effect was greatest at P30, with reduced changes in PV+ inhibition at later ages, suggesting a shift in the circuit mechanisms of learning related plasticity later in life.

Methods

Stereotactic injections

Animal protocols were approved by the Institutional Animal Care and Use Committee at the University of Pittsburgh. Mice of both sexes were used. Mice were held in standard housing cages with ad libitum access to food and water. Mice were housed in standard mouse caging without running wheels to minimize prior exposure to a treadmill, as running wheel exposure might shift the learning curve (Buitrago 2004). Injections were made with glass pipette (Drummond) using a custom-made positive displacement system (Narashige). In order to label and optogenetically stimulate specific interneurons, Cre driver mouse lines (PV-Cre, JAX 008069; and SOM-Cre, JAX 013044) were crossed with Ai32(lsl-ChR2-EYFP, JAX 012569). lsl-ReaChR-mCitrine mice (JAX 026294) were used in some pilot experiments. Offspring were then injected with CaMPARI2 (pAAV_hsyn_NES-his-CaMPARI2-WPRE-SV40, Addgene 101060) perinatally at postnatal day (P) 0-3. Due to the age of the animals, pups were cryoanesthetized on ice and placed in a custom clay mold to position the animal during the injection while maintaining low temperature. Stereotaxic coordinates for M1 differ from the adult and Bregma is invisible above the skin. To overcome this, confluence of sinuses, which approximately corresponds to Lambda, was used for alignment. The injection was made at 2100 µm anterior and 1000 µm lateral at two depths – 695 µm and 665 µm – 50 nl each.

Clear Skull and LED mounting

Once animals approach the developmental age for testing, the skull was cleared 3-5 days prior to rotarod training to minimize tissue damage. The mice were anesthetized with a O_2 rate of 1 L/min and 2.5%-3.0% isoflurane. During surgery, Buprenorphine (0.1mg/kg) and Ketoprofen (4 mg/kg) were administered intraperitoneally for analgesia. The scalp and periosterum of the skull were removed. The CaMPARI2 injection site was visible through the skull by illuminating the exposed skull with a Nightsea system (SFA Stereo Microscope Fluorescence Adapter) and the boundary of the injection site was delineated using a marker. The skull was scored with scalpel to enhance the adherence of the cap. A layer of cyanoacrylate (~1-2 mm) was applied and a headplate was

positioned above the cerebellum. Clear dental cement was applied over the skull before the cyanoacrylate was fully dry. The day before the training day, clear nail polish was applied and a high-power UV-LED (405 nm) was placed on top of the injection site (Mouser, 604-ATDS3534UV405B). The rest of the skull cap was sealed with black silicone. Because the headcap came unattached more readily in young mice, the younger age group was shifted from P15 to P20 because the LED adhered better at this age. Mice where the headcap was removed were taken out of the study.

Mice and Behavior

Animals were trained on an accelerating rotarod. The rotation accelerated uniformly from 0 to 90 RPM in 3 minutes. Animals performed 20 trials in a session and only one session per day. Animals were trained for 5 consecutive days, except those sacrificed earlier for brain slice experiments. The custom-designed rotarod (Figure S1) was built from clear plexiglass. A stepper motor (uxcell) was connected to a clear rod and was controlled by an Arduino board. Panels dividing the lanes of the rotarod were able to slide along the rod to adjust the width of the running lane to the size of the animal running on the rotarod. At the bottom, a high-speed camera (FLIR Blackfly S USB3) was mounted to record the animal during the task. Six age groups were tested: postnatal day(P) 15-20, P30, P45, P60, P90, and P120. For the animals expressing CaMPARI2, UV-LED light was delivered (0.1s ON, 0.9s OFF) during rotarod training. Once the animal fell from the rod, LED stimulation was terminated. Time to fall was measured throughout all trials. The animal's performance was recorded using high-speed camera at 200 frames per second. The youngest age group includes P15-20. While animals around P15 become ambulatory and can stay on the rotarod, this age was not ideal for rotarod training. First, the skull at P15 is still not mature enough to mount LED. Second, because animals at this age are not weaned from the parents, oftentimes the LED mount was damaged by the parents. Therefore, P20 animals became more suitable to test in both the rotarod task and electrophysiology.

Behavioral Analysis

Improvement measured in time to fall was calculated by taking the average of trials 1-3 and subtracting it from the average of trials 11-13 (Figure 1C). A one-way ANOVA was performed to compare the improvement in six age groups. Tukey's multiple comparison test was used after the ANOVA. For single comparisons (muscimol), t-test was used. The same analysis was used to compare the baseline locomotion. To determine the difference in weights between male and female within an age group, t-test was used. We focused on P20-60 animals, which correspond with best ages of the animals recorded for slice electrophysiology. The body positions of the animals were estimated using DeepLabCut [48]. The nose, right front paw, left front paw, right hind paw, left hind paw and base of the tail were annotated manually for training and subsequently tracked for analysis. Estimated data points with likelihood less than 0.95 were excluded from analysis. To analyze the changes in the position of a single paw, steps were detected using custom software. The start and end of a step were converted to location relative to the front (1.0) and rear (0.0) edge of the rotarod (Figure 2). The step length was calculated by measuring the distance between the step start and end. To analyze the changes in the gait pattern, the phase of the left and right paws (Figure 3) was determined by comparing location and timing of one step between the corresponding steps with the opposite paw, for example where a left hind paw (LHP) step occurred between two right hind paw (RHP) steps. For the gait analysis, one-way ANOVA was performed to compare the gait phases between the deciles and the trials. Tukey's multiple comparison test was used after the ANOVA. Comparison between a decile and trial of P20 to the corresponding decile of P30, P45 and P60 were made using t-test.

Muscimol inactivation

To determine whether M1 is necessary to learn the accelerating rotarod task, M1 was pharmacologically inactivated. Muscimol (5 mg/ml, 40 nL per hemisphere) or saline was injected into forelimb M1 bilaterally in animals P30-45 (600 µm anterior, 1500 µm lateral, 500 and 800 µm depth, with 20 nL at each depth). 40 minutes following removal from anesthesia, the animals were tested on the accelerating rotarod.

Fluorescence Analysis

Using ImageJ, red and green fluorescence were measured for the injection site and the recorded cells. Mean fluorescence was calculated by dividing the sum of the count multiplied by their histogram value with the sum of total counts. Photoconversion ratio was calculated by dividing the red fluorescence mean by the green fluorescence mean. For the pair of cells recorded, photoconversion ratio between the cells were compared and the cells with higher photoconversion ratio was considered as task-active while the other cells in each pair with lower photoconversion ratio was considered as task-inactive.

Electrophysiology

After completing rotarod training, mice were anesthetized with isoflurane, and the brains were extracted in ice-cold choline chloride based cutting solution (in mM: 25 $NaHCO_3$, 25 D-glucose, 1.25 NaH_2PO_4, 2.5 KCl, 7 $MgCl_2$, 0.5 $CaCl_2$, 3.1 Sodium Pyruvate, 11.6 Sodium Ascorbate, 110 Choline Chloride). Then the brains were sectioned coronally at 300 µm, using a vibratome in choline chloride based cutting solution. Sections were moved to artificial cerebrospinal fluid (aCSF in mM: 127 NaCl, 25 $NaHCO_3$, 25 D-Glucose, 2.5 KCl, 2 $CaCl_2$, 1.25 NaH_2PO_4, 1 $MgCl_2$), then transferred into aCSF at 38°C for 30 minutes then at room temperature for 30 minutes. Patch pipettes were pulled from borosilicate glass. The pipette was filled with cesium based intracellular solution (in mM: 35 CsF, 100 CsCl, 10 EGTA, and 10 HEPES). Recordings were performed at room temperature (22 °C), amplified by an Axopatch 700B amplifier (Molecular devices) and acquired at 10KHz in WaveSurfer, open-source software, (https://wavesurfer.janelia.org). Neurons were selected across the thickness of L5. The cell was voltage clamped at +40 mV. To elicit IPSCs, blue LED stimulation (470 nm) was delivered for 1, 2, and 5 ms with 20 second intervals in between each sweep for recovery. The cycle was repeated three times.

Electrophysiology Analysis

Electrophysiology data were low-pass filtered (1kHz). The three traces were averaged. IPSCs were measured when they exceeded a threshold of greater than 5x standard deviation from the baseline. Cells with membrane capacitance (Cm) below 70 pF were

excluded from analysis. Neurons expressing CaMPARI2 (red, task-active cells; green, task-inactive cells) were targeted for recordings. To compare neurons within a slice, nearby task-active (red) and task-inactive cells in the same high-power (60x field of view) were recorded. The peak IPSC amplitude of task-active and task-inactive cells were compared using Wilcoxon rank sum test. IPSCs of task-active cells were normalized to their partner inactive cells and the ratio and the ratio was analyzed using Wilcoxon rank sum test.

Figure Legends

Figure 1 | Rotarod skill acquisition plateaus around P30-P60 on training day 1.
(A) Schematic of rotarod task with high speed videography and barriers to create the running lane during a trial. (B) Video frame of mouse during running. Paw positions (LFP, left front paw; LHP, left hind paw; RFP, right front paw; RHP, right hind paw) and the nose and tail base are tracked using DeepLabCut. (C) Learning curve during 20 trials on training day 1 (TD1). Six colors represent the six ages tested (P15-20, P30, P45, P60, P90, and P120). Gray bars represent time windows used for early and late performance to assess TD1 improvement. (D) Improvement (in seconds) in time to fall during TD1 for six age groups. Mean+/- SEM. N=63, 92, 60 63, 27, 12. (E) Improvement (in seconds) in time to fall during TD1 for six age groups, subdivided by male (blue) and female (red). Mean+/- SEM.(F) Improvement (in seconds) in time to fall during five training days. Gray vertical lines divide the days. Mean+/- SEM. (G) The effect of M1 inactivation by bilateral muscimol injection on rotarod skill acquisition compared to saline injected controls. N=5 (control); N=9 (muscimol). Mean+/- SEM. Significance: *, $p<0.05$; **, $p<0.01$; ***, $p<0.001$.

Figure 2 | Tracking step kinematics during rotarod training.
(A) Schematic of rotarod task with video frame of tracked mouse. (B) Cartoon of tracked image frame illustrating location of the mouse paws (LFP, left front paw; LHP, left hind paw; RFP, right front paw; RHP, right hind paw) and the nose and tail base using DeepLabCut. The rotarod and direction of motion are indicated, with the front and rear ends of the rod serving as 0.0 and 1.0 in normalized coordinates. At bottom, coordinates for the step start, step end, and step length are plotted to illustrate how they are determined. (C) Plot of the x-position of a single paw (LHP, left) or all paws (right) during a trial. Time given in frames (converted to seconds with example timebar). (D) Expansion of paw tracker showing step detection. Steps (red) are automatically detected (see methods). Step start (green), step end (black), and step length are then calculated. (E) Step length versus time to fall for the left front paw, plotted for all ages combined (red) and individual ages (20 and above). Data are fit to a line and the linear

fit compared at right. Summary plots include step length versus time to fall for the right front paw, left hind paw, and right hind paw (far right). (F) Step end point presented similarly to step length.

Figure 3 | Gait pattern changes with age and training.

(A) Schematic of rotarod task with video frame of tracked mouse. (B) Cartoon of tracked image frame illustrating location of the mouse paws (LFP, left front paw; LHP, left hind paw; RFP, right front paw; RHP, right hind paw) and the nose and tail base using DeepLabCut. The rotarod and direction of motion are indicated, with the front and rear ends of the rod serving as 0.0 and 1.0 in normalized coordinates. At bottom, coordinates for the step start, step end, and step length are plotted to illustrate how they are determined. (C) Plot of the x-position of a single paw (LHP, left) or all paws (right) during a trial. Time given in frames (converted to seconds with example timebar). (D) Expansion of paw tracker showing step detection. Steps (red) are automatically detected (see methods). Step start (green), step end (black), and step length are then calculated. (E) Step length versus time to fall for the left front paw, plotted for all ages combined (red) and individual ages (20 and above). Data are fit to a line and the linear fit compared at right. Summary plots include step length versus time to fall for the right front paw, left hind paw, and right hind paw (far right). (F) Step end point presented similarly to step length. Significance: *, $p<0.05$; **, $p<0.01$; ***, $p<0.001$.

Figure 4 | P-values for the gait analysis.

(A) Due to variations in the number of steps, the number of steps in a trial were divided into deciles to facilitate the comparison of average step phases across trials and age groups. The average step phase value for each age for front and hind limbs is plotted. (B) The P-value plot of deciles compares the first decile of trials 1-20 to rest of the deciles (2-9) for each trial. The top row compares front paws at four ages and the bottom row compares hind paws. Non-significant p-values are purple; p-values < 0.05 are as shown in the lookup table. (C) The P-value plot comparing across trials compares each decile from trials 2-20 with the corresponding decile from trial 1. The top row compares front paws at four ages and the bottom row compares hind paws. For

instance, the front paw in P20 Decile 3 from trial 3 is compared to Decile 3 from trial 1. Non-significant p-values are purple; p-values < 0.05 are as shown in the lookup table. (D) The P-value plot of deciles compared across ages assess P20 versus P30, P45, and P60 groups for 20 trials. Each individual graph represents the comparison between the four age groups for a given trial. The X-axis denotes deciles, with a specific trial's decile being compared to the corresponding decile of the P20 group. For example, the front paw in P30 Decile 9 is compared to P20 Decile 9 in the trial 1 graph, and if significantly different, it is indicated by a bump in the y-axis. Significance: *; p<0.05. **;p<0.01, ***;p<0.001.

Figure 5 | Schematic of CaMPARI2 manipulation.

(A) AAV expresses CaMPARI2 in M1 in PVcre+/-;Ai32+/- or SOMcre+/-;Ai32+/- mice. (B,C) CaMPARI2-expressing cells are photoconverted to red by a skull mounted UV LED. (D) Example images of a slice after photoconversion during rotarod. Green arrowheads mark green neurons not photoconverted (task-inactive) to red; red arrowheads mark red neurons (task-active). (E) Example traces from task-inactive (green) and task-active (red) neurons after LED stimulation of PV+ cells. (F) Photoconversion ratio is calculated by dividing red fluorescence over green fluorescence. Animals showed greater photoconversion ratio after rotarod training (grey) compared to the control animals that were permitted to move freely in the rotarod chamber floor (white). Significance: *; p<0.05.

Figure 6 l IPSCs recorded in task-active (RFP+) vs. task-inactive cells (GFP+) after stimulating PV+ interneurons

(A-E) Scatter plot of IPSC responses in pairs of task-active (red) and task-inactive (green) cells in P20 (A), P30 (B), P45 (C), P60(D) and across all age groups (E). Solid line is the geometric mean of the pair responses. Dotted line is the line of equality (x=y). (F) Slopes of geometric mean across all ages plotted together. (G-K) Ratio of responses of task-active cells to their partner task-inactive cells after PV+ stimulation in P20 (G), P30 (H), P45 (I), P60 (J) and across all age groups (K). Significance: *, p<0.05; **,

p<0.01; ***, p<0.001. (Also indicated with red arrows in (A-E). (L) Schematic of the genetic strategy for testing PV output to M1 pyramidal neurons

Figure 7 l IPSCs recorded in task-active (RFP+) vs. task-inactive cells (GFP+) after stimulating SOM+ interneurons

(A-E) Scatter plot of IPSC responses in pairs of task-active (red) and task-inactive (green) cells in P20 (A), P30 (B), P45 (C), P60(D) and across all age groups (E). Solid line is the geometric mean of the pair responses. Dotted line is the line of equality (x=y). (F) Schematic of the genetic strategy for testing SOM output to M1 pyramidal neurons. (G-K) Ratio of responses of task-active cells to their partner task-inactive cells after SOM+ stimulation in P20 (G), P30 (H), P45 (I), P60 (J) and across all age groups (K).

Supplementary Information

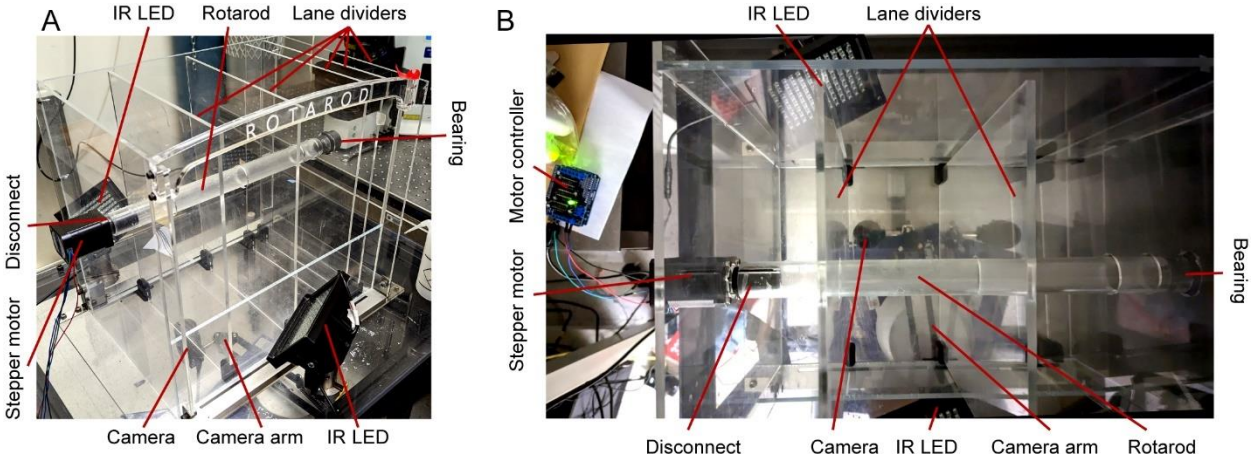

Figure S1 | Rotarod design

(A) Image of a clear plexiglass rotarod with high speed video. Steeper motor and camera run by computer adjacent to the operator. Multiple lanes are possible (divided by moveable lane dividers) to simultaneously run multiple mice (two lanes in the camera field of view). Infrared (IR) LEDs used for illumination during behavioral training. (B) Overhead view of the apparatus. Lane dividers opened further than during trials to illustrate capacity for sliding.

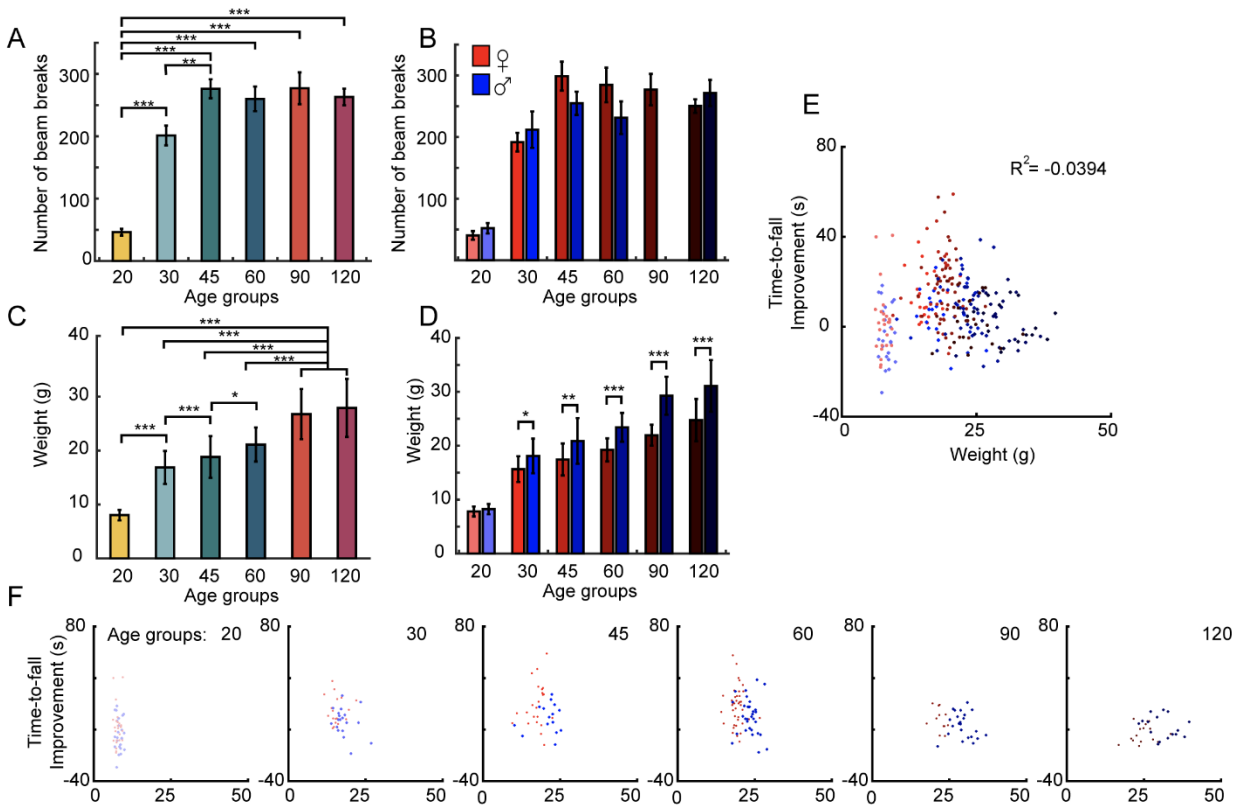

Figure S2 | Developmental changes in mobility and weight do not account for rotarod performance

(A) Measurement of home cage walking (beam breaks) used to assess motility across developmental ages. (B) Home cage motility quantified by sex across ages. Red/blue is used to designate sex (red, female; blue, male), with brightness used to indicate age. The same color scheme is used in D-E. (C-D) Changes in weight across developmental ages, quantified for all mice or by sex. Male mice weigh more than female mice at ages older than P30. (E) Plot comparing the first training day (TD1) time-to-fall improvement versus weight. Red/blue color code is used to indicate age and sex. Linear fit is relatively poor (R^2=-0.04). Significance: *, p<0.05; **, p<0.01; ***, p<0.001.

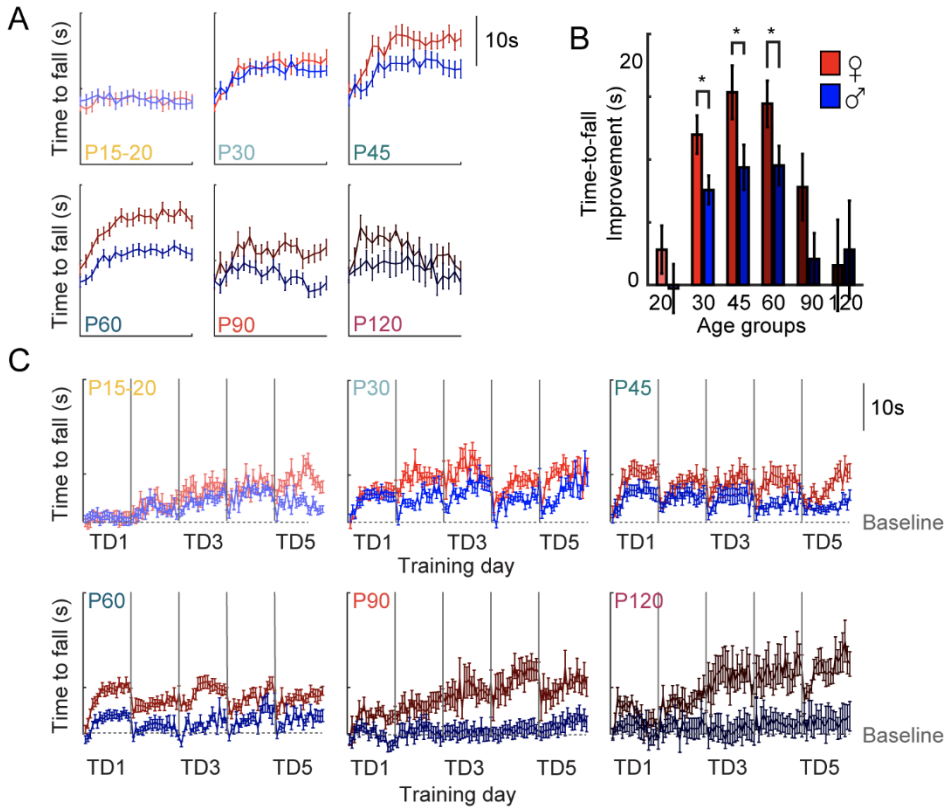

Figure S3 | Developmental changes in rotarod performance plotted for male and female

(A) Measurement of training day 1 (TD1) performance, separated by male (blue) and female (red). (B) Summary of time-to-fall improvement, plotted as in Figure 1. (C) Measurement of rotarod performance across all training days, separated by male (blue) and female (red). Significance: *, p<0.05; **, p<0.01; ***, p<0.001.

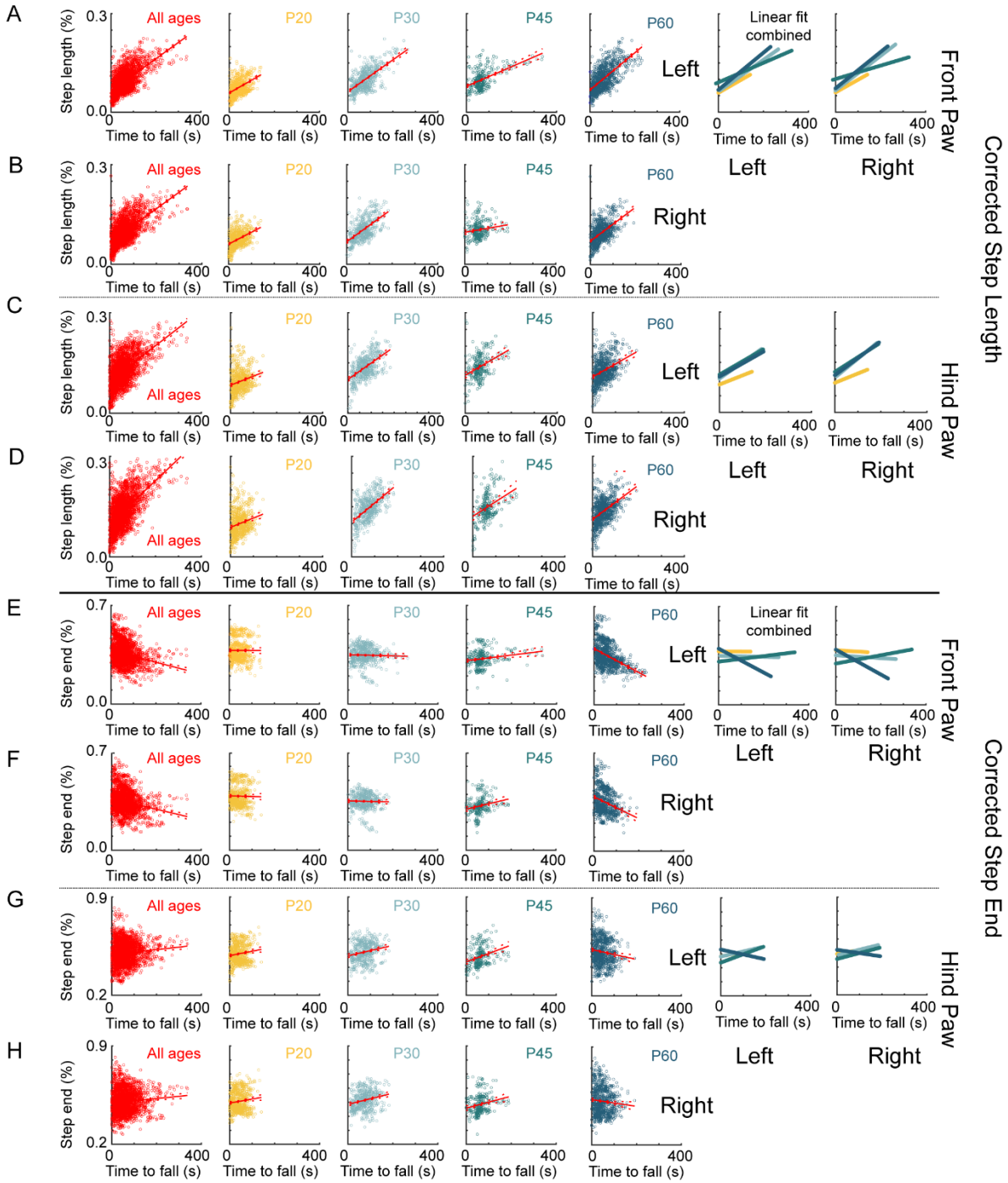

Figure S4 | Step kinematics across ages and limbs

(A) Step length versus time to fall for the left front paw, plotted for all ages combined (red) and individual ages (20 and above). Data are fit to a line and the linear fit compared at right. (B-D) Step length versus time to fall for the right front paw (B), left hind paw (C), and right hind paw (D). (E-H) Step end point presented similarly to step length.

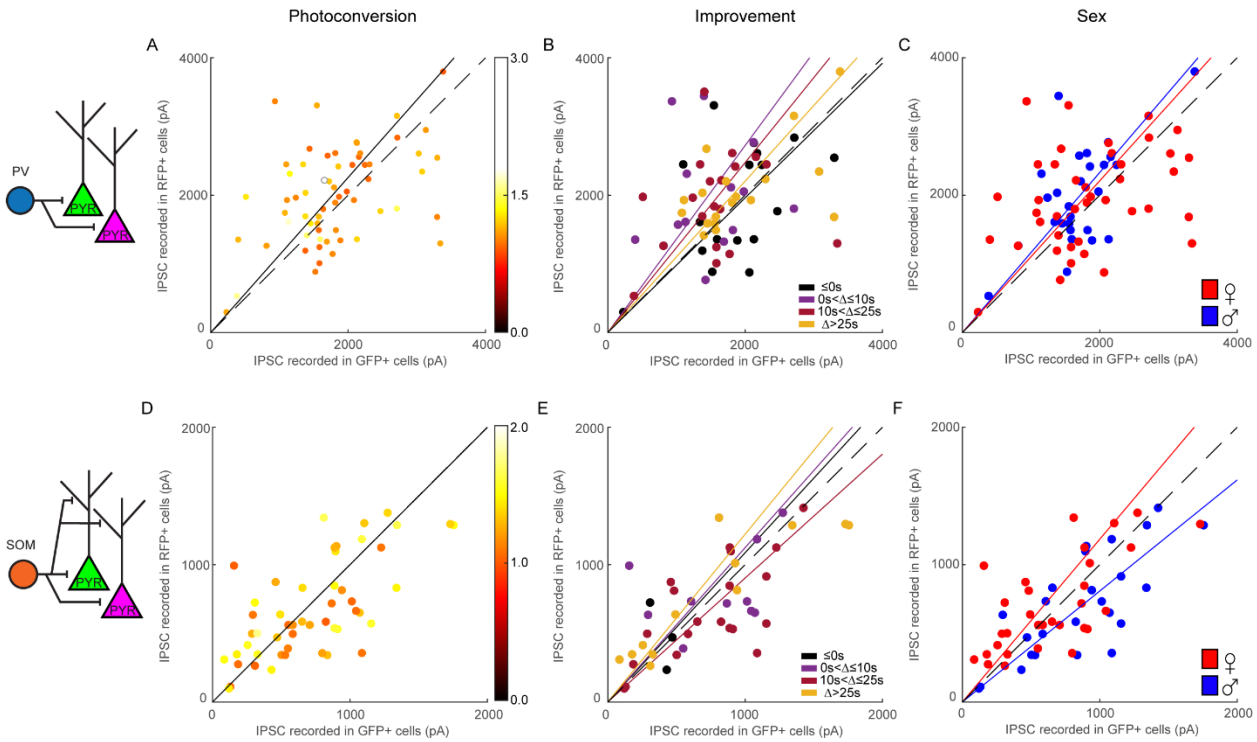

Figure S5 I Additional factors considered for the pair recordings

To determine whether other factors could potentially affect the pair recordings, we replotted Figure 5 and 6, using the color of the data representing a third variable. The degree of photoconversion was assessed by plotting by the red/green fluorescence ratio for the recordings from PV+ (A) and SOM+ (D) stimulation. Higher the ratio is, the greater the difference in photoconversion between the pair. In addition, four different improvement magnitudes were plotted by four different colors for the recordings from PV+ (B) and SOM+ (E) stimulation. The geometric mean of the respective improvement groups was plotted in solid line of the same color scheme. Lastly, male and female were plotted in red and blue for the recordings from PV+ (C) and SOM+ (F) stimulation. The geometric mean of the respective sex was plotted in solid line of the same color scheme.

References

1. Chen, S. X., Kim, A. N., Peters, A. J. & Komiyama, T. Subtype-specific plasticity of inhibitory circuits in motor cortex during motor learning. *Nat Neurosci* **18**, 1109–15 (2015).
2. Hensch, T. K. Critical period plasticity in local cortical circuits. *Nature Reviews Neuroscience* vol. 6 877–888 Preprint at https://doi.org/10.1038/nrn1787 (2005).
3. Erzurumlu, R. S. & Gaspar, P. Development and critical period plasticity of the barrel cortex. *European Journal of Neuroscience* (2012) doi:10.1111/j.1460-9568.2012.08075.x.
4. Hooks, B. M. & Chen, C. Circuitry Underlying Experience-Dependent Plasticity in the Mouse Visual System. *Neuron* (2020) doi:10.1016/j.neuron.2020.08.004.
5. Kawai, R. *et al.* Motor Cortex Is Required for Learning but Not for Executing a Motor Skill. *Neuron* **86**, 800–812 (2015).
6. Sauerbrei, B. A. *et al.* Cortical pattern generation during dexterous movement is input-driven. *Nature* **577**, 386–391 (2020).
7. Papale, A. E. & Hooks, B. M. Circuit Changes in Motor Cortex During Motor Skill Learning. *Neuroscience* **368**, 283–297 (2018).
8. Knudsen, E. I. & Knudsen, P. F. Sensitive and critical periods for visual calibration of sound localization by barn owls. *Journal of Neuroscience* **10**, 222–232 (1990).
9. Gordon, J. A. & Stryker, M. P. Experience-dependent plasticity of binocular responses in the primary visual cortex of the mouse. *J Neurosci* **16**, 3274–3286 (1996).
10. Van Der Loos, H. & Woolsey, T. A. Somatosensory cortex: structural alterations following early injury to sense organs. *Science* **179**, 395–398 (1973).
11. Costa, R. M., Cohen, D. & Nicolelis, M. A. L. Differential Corticostriatal Plasticity during Fast and Slow Motor Skill Learning in Mice. *Current Biology* **14**, 1124–1134 (2004).
12. Dombeck, D. A., Graziano, M. S. & Tank, D. W. Functional Clustering of Neurons in Motor Cortex Determined by Cellular Resolution Imaging in Awake Behaving Mice. *Journal of Neuroscience* **29**, 13751–13760 (2009).
13. Peters, A. J., Chen, S. X. & Komiyama, T. Emergence of reproducible spatiotemporal activity during motor learning. *Nature* **510**, 263–267 (2014).

14. Hira, R. *et al.* Spatiotemporal dynamics of functional clusters of neurons in the mouse motor cortex during a voluntary movement. *J Neurosci* **33**, 1377–1390 (2013).
15. Yang, G., Pan, F. & Gan, W.-B. Stably maintained dendritic spines are associated with lifelong memories. *Nature* **462**, 920–4 (2009).
16. Yang, G. *et al.* Sleep promotes branch-specific formation of dendritic spines after learning. *Science* **344**, 1173–8 (2014).
17. Weiler, N., Wood, L., Yu, J., Solla, S. A. & Shepherd, G. M. G. Top-down laminar organization of the excitatory network in motor cortex. *Nat Neurosci* **11**, 360–366 (2008).
18. Mao, T. *et al.* Long-Range Neuronal Circuits Underlying the Interaction between Sensory and Motor Cortex. *Neuron* **72**, 111–123 (2011).
19. Hooks, B. M. *et al.* Organization of cortical and thalamic input to pyramidal neurons in mouse motor cortex. *Journal of Neuroscience* (2013) doi:10.1523/JNEUROSCI.4338-12.2013.
20. Jacobs, K. M. & Donoghue, J. P. Reshaping the cortical motor map by unmasking latent intracortical connections. *Science* **251**, 944–947 (1991).
21. Rioult-Pedotti, M. S., Friedman, D. & Donoghue, J. P. Learning-induced LTP in neocortex. *Science* **290**, 533–536 (2000).
22. Kaneko, T., Caria, M. A. & Asanuma, H. Information processing within the motor cortex. II. Intracortical connections between neurons receiving somatosensory cortical input and motor output neurons of the cortex. *J Comp Neurol* **345**, 172–184 (1994).
23. Southwell, D. G., Froemke, R. C., Alvarez-Buylla, A., Stryker, M. P. & Gandhi, S. P. Cortical plasticity induced by inhibitory neuron transplantation. *Science (1979)* (2010) doi:10.1126/science.1183962.
24. Tang, Y., Stryker, M. P., Alvarez-Buylla, A. & Espinosa, J. S. Cortical plasticity induced by transplantation of embryonic somatostatin or parvalbumin interneurons. *Proc Natl Acad Sci U S A* (2014) doi:10.1073/pnas.1421844112.
25. Bachtiar, V. & Stagg, C. J. The role of inhibition in human motor cortical plasticity. *Neuroscience* **278**, 93–104 (2014).
26. Kolasinski, J. *et al.* The dynamics of cortical GABA in human motor learning. *J Physiol* **597**, 271–282 (2019).

27. Blicher, J. U. *et al.* GABA levels are decreased after stroke and GABA changes during rehabilitation correlate with motor improvement. *Neurorehabil Neural Repair* **29**, 278–286 (2015).
28. Alia, C. *et al.* Reducing GABA A-mediated inhibition improves forelimb motor function after focal cortical stroke in mice. *Sci Rep* (2016) doi:10.1038/srep37823.
29. Kida, H. *et al.* Motor training promotes both synaptic and intrinsic plasticity of layer V pyramidal neurons in the primary motor cortex. *J Physiol* **601**, 335–353 (2023).
30. Kida, H. *et al.* Motor Training Promotes Both Synaptic and Intrinsic Plasticity of Layer II/III Pyramidal Neurons in the Primary Motor Cortex. *Cerebral Cortex (New York, NY)* **26**, 3494 (2016).
31. Rudy, B., Fishell, G., Lee, S. & Hjerling-Leffler, J. Three groups of interneurons account for nearly 100% of neocortical GABAergic neurons. *Dev Neurobiol* **71**, 45–61 (2011).
32. Tremblay, R., Lee, S. & Rudy, B. GABAergic Interneurons in the Neocortex: From Cellular Properties to Circuits. *Neuron* **91**, 260–92 (2016).
33. Pfeffer, C. K., Xue, M., He, M., Huang, Z. J. & Scanziani, M. Inhibition of inhibition in visual cortex: the logic of connections between molecularly distinct interneurons. *Nat Neurosci* **16**, 1068–1076 (2013).
34. Kawaguchi, Y. & Kubota, Y. Neurochemical features and synaptic connections of large physiologically-identified GABAergic cells in the rat frontal cortex. *Neuroscience* **85**, 677–701 (1998).
35. Somogyi, P., Tamás, G., Lujan, R. & Buhl, E. H. Salient features of synaptic organisation in the cerebral cortex. *Brain Res Rev* **26**, 113–135 (1998).
36. Xue, M., Atallah, B. V. & Scanziani, M. Equalizing excitation–inhibition ratios across visual cortical neurons. *Nature* **511**, 596–600 (2014).
37. Kuhlman, S. J. *et al.* A disinhibitory microcircuit initiates critical-period plasticity in the visual cortex. *Nature* **501**, 543–546 (2013).
38. Friel, K., Chakrabarty, S., Kuo, H. C. & Martin, J. Using Motor Behavior during an Early Critical Period to Restore Skilled Limb Movement after Damage to the Corticospinal System during Development. *Journal of Neuroscience* **32**, 9265–9276 (2012).
39. Walton, K. D., Lieberman, D., Llinás, A., Begin, M. & Llinás, R. R. Identification of a critical period for motor development in neonatal rats. *Neuroscience* **51**, 763–767 (1992).

40. Adler, A., Zhao, R., Shin, M. E., Yasuda, R. & Gan, W.-B. Somatostatin-Expressing Interneurons Enable and Maintain Learning-Dependent Sequential Activation of Pyramidal Neurons. *Neuron* **102**, 202-216.e7 (2019).
41. Ren, C. *et al.* Global and subtype-specific modulation of cortical inhibitory neurons regulated by acetylcholine during motor learning. *Neuron* **110**, 2334-2350.e8 (2022).
42. Moeyaert, B. *et al.* Improved methods for marking active neuron populations. *Nat Commun* **9**, 4440 (2018).
43. Grillner, S. & Wallén, P. Central pattern generators for locomotion, with special reference to vertebrates. *Annu Rev Neurosci* **8**, 233–261 (1985).
44. Buitrago, M. M., Schulz, J. B., Dichgans, J. & Luft, A. R. Short and long-term motor skill learning in an accelerated rotarod training paradigm. *Neurobiol Learn Mem* **81**, 211–216 (2004).
45. Greenwood, B. N. & Fleshner, M. Voluntary Wheel Running: A Useful Rodent Model for Investigating the Mechanisms of Stress Robustness and Neural Circuits of Exercise Motivation. *Curr Opin Behav Sci* **28**, 78 (2019).
46. Sherwin, C. M. Voluntary wheel running: a review and novel interpretation. *Anim Behav* **56**, 11–27 (1998).
47. Jain, A., Huang, G. Z. & Woolley, C. S. Latent Sex Differences in Molecular Signaling That Underlies Excitatory Synaptic Potentiation in the Hippocampus. *Journal of Neuroscience* **39**, 1552–1565 (2019).
48. Mathis, A. *et al.* DeepLabCut: markerless pose estimation of user-defined body parts with deep learning. *Nat Neurosci* **21**, 1281–1289 (2018).
49. Huang, Y., Zhang, X. & Li, W. Involvement of primary somatosensory cortex in motor learning and task execution. *Neurosci Lett* **828**, 137753 (2024).
50. Iturralde, P. A. & Torres-Oviedo, G. Corrective Muscle Activity Reveals Subject-Specific Sensorimotor Recalibration. *eNeuro* **6**, (2019).
51. Donato, F., Rompani, S. B. & Caroni, P. Parvalbumin-expressing basket-cell network plasticity induced by experience regulates adult learning. *Nature* (2013) doi:10.1038/nature12866.
52. Goz, R. U. & Hooks, B. M. Correlated Somatosensory Input in Parvalbumin/Pyramidal Cells in Mouse Motor Cortex. *eNeuro* **10**, 1–18 (2023).
53. Znamenskiy, P. *et al.* Functional specificity of recurrent inhibition in visual cortex. (2024) doi:10.1016/j.neuron.2023.12.013.

54. Isomura, Y., Harukuni, R., Takekawa, T., Aizawa, H. & Fukai, T. Microcircuitry coordination of cortical motor information in self-initiation of voluntary movements. *Nature Neuroscience 2009 12:12* **12**, 1586–1593 (2009).
55. Sohal, V. S., Zhang, F., Yizhar, O. & Deisseroth, K. Parvalbumin neurons and gamma rhythms enhance cortical circuit performance. *Nature* **459**, 698 (2009).
56. Cardin, J. A. *et al.* Driving fast-spiking cells induces gamma rhythm and controls sensory responses. *Nature* **459**, 663 (2009).
57. Howard, M. W. *et al.* Gamma oscillations correlate with working memory load in humans. *Cereb Cortex* **13**, 1369–1374 (2003).
58. Lewis, D. A., Hashimoto, T. & Volk, D. W. Cortical inhibitory neurons and schizophrenia. *Nature Reviews Neuroscience 2005 6:4* **6**, 312–324 (2005).
59. Nowak, M. *et al.* Driving Human Motor Cortical Oscillations Leads to Behaviorally Relevant Changes in Local GABAA Inhibition: A tACS-TMS Study. *Journal of Neuroscience* **37**, 4481–4492 (2017).
60. Estebanez, L., Hoffmann, D., Voigt, B. C. & Poulet, J. F. A. Parvalbumin-Expressing GABAergic Neurons in Primary Motor Cortex Signal Reaching. *Cell Rep* **20**, 308–318 (2017).
61. Chattopadhyaya, B. *et al.* Experience and Activity-Dependent Maturation of Perisomatic GABAergic Innervation in Primary Visual Cortex during a Postnatal Critical Period. *Journal of Neuroscience* **24**, 9598–9611 (2004).
62. Miyamae, T., Chen, K., Lewis, D. A. & Gonzalez-Burgos, G. Distinct Physiological Maturation of Parvalbumin-Positive Neuron Subtypes in Mouse Prefrontal Cortex. *The Journal of Neuroscience* **37**, 4883 (2017).
63. Canetta, S. E. *et al.* Mature parvalbumin interneuron function in prefrontal cortex requires activity during a postnatal sensitive period. *Elife* **11**, (2022).
64. Hwang, E. J., Dahlen, P. J. E., Mukundan, P. M. & Komiyama, T. Disengagement of Motor Cortex during Long-Term Learning Tracks the Performance Level of Learned Movements. *Journal of Neuroscience* **41**, 7029–7047 (2021).
65. Yang, J. *et al.* Functionally distinct NPAS4-expressing somatostatin interneuron ensembles critical for motor skill learning. *Neuron* **110**, 3339-3355.e8 (2022).
66. Yang, J. *et al.* Functionally distinct NPAS4-expressing somatostatin interneuron ensembles critical for motor skill learning Highlights d Motor learning selectively induces NPAS4 expression in SST-INs in M1 d Cell-type specific KO of Npas4 in SST-INs of M1 in mice impairs motor learning d NPAS4 + SST-INs exhibited lower

activity during task-related movements d NPAS4 re-expression maintains the functionally distinct SST-INs throughout learning. doi:10.1016/j.neuron.2022.08.018.

67. Shepherd, G. M. G. Corticostriatal connectivity and its role in disease. *Nature Reviews Neuroscience* vol. 14 278–291 Preprint at https://doi.org/10.1038/nrn3469 (2013).

68. Park, J. *et al.* Motor cortical output for skilled forelimb movement is selectively distributed across projection neuron classes. *Sci Adv* **8**, (2022).

69. Currie, S. P. *et al.* Movement-specific signaling is differentially distributed across motor cortex layer 5 projection neuron classes. (2022) doi:10.1016/j.celrep.2022.110801.

70. Li, N., Chen, T. W., Guo, Z. V., Gerfen, C. R. & Svoboda, K. A motor cortex circuit for motor planning and movement. *Nature* **519**, 51–56 (2015).

71. Soma, S. *et al.* Systems/Circuits Distinct Laterality in Forelimb-Movement Representations of Rat Primary and Secondary Motor Cortical Neurons with Intratelencephalic and Pyramidal Tract Projections. (2017) doi:10.1523/JNEUROSCI.1188-17.2017.

72. Shinotsuka, T., Tanaka, Y. R., Terada, S. I., Hatano, N. & Matsuzaki, M. Layer 5 Intratelencephalic Neurons in the Motor Cortex Stably Encode Skilled Movement. *J Neurosci* **43**, 7130–7148 (2023).